



HAL
open science

Search for supersymmetric partners of top and bottom quarks at $\sqrt{s} = 189$ GeV

P. Abreu, W. Adam, T. Adye, P. Adzic, I. Ajinenko, Z. Albrecht, T. Alderweireld, G D. Alekseev, R. Alemany, T. Allmendinger, et al.

► **To cite this version:**

P. Abreu, W. Adam, T. Adye, P. Adzic, I. Ajinenko, et al.. Search for supersymmetric partners of top and bottom quarks at $\sqrt{s} = 189$ GeV. Physics Letters B, 2000, 496, pp.59-75. 10.1016/S0370-2693(00)01275-2 . in2p3-00007893

HAL Id: in2p3-00007893

<https://hal.in2p3.fr/in2p3-00007893>

Submitted on 11 Jan 2001

HAL is a multi-disciplinary open access archive for the deposit and dissemination of scientific research documents, whether they are published or not. The documents may come from teaching and research institutions in France or abroad, or from public or private research centers.

L'archive ouverte pluridisciplinaire **HAL**, est destinée au dépôt et à la diffusion de documents scientifiques de niveau recherche, publiés ou non, émanant des établissements d'enseignement et de recherche français ou étrangers, des laboratoires publics ou privés.

Search for supersymmetric partners of top and bottom quarks at $\sqrt{s} = 189 \text{ GeV}$

DELPHI Collaboration

Abstract

Searches for supersymmetric partners of top and bottom quarks are presented using data taken by the DELPHI experiment at LEP in 1997 and 1998. No deviations from standard model expectations are observed in these data sets, which are taken at centre-of-mass energies of 183 GeV and 189 GeV and correspond to integrated luminosities of 54 pb^{-1} and 158 pb^{-1} . These results are used in combination with those obtained by DELPHI at lower centre-of-mass energies to exclude regions in the squark-neutralino mass plane at 95% confidence level.

(Submitted to Phys.Lett.B)

P.Abreu²², W.Adam⁵², T.Adye³⁸, P.Adzic¹², I.Ajinenko⁴⁴, Z.Albrecht¹⁸, T.Alderweireld², G.D.Alekseev¹⁷, R.Aleman⁵¹, T.Allmendinger¹⁸, P.P.Allport²³, S.Almeheid²⁵, U.Amaldi^{9,29}, N.Amapane⁴⁷, S.Amato⁴⁹, E.G.Anassontzis³, P.Andersson⁴⁶, A.Andrezza⁹, S.Andringa²², P.Antilogus²⁶, W-D.Apel¹⁸, Y.Arnoud⁹, B.Åsman⁴⁶, J-E.Augustin²⁶, A.Augustinus⁹, P.Baillon⁹, A.Ballestrero⁴⁷, P.Bambade²⁰, F.Barao²², G.Barbiellini⁴⁸, R.Barbier²⁶, D.Y.Bardin¹⁷, G.Barker¹⁸, A.Baroncelli⁴⁰, M.Battaglia¹⁶, M.Baubillier²⁴, K-H.Becks⁵⁴, M.Begalli⁶, A.Behrmann⁵⁴, P.Beilliere⁸, Yu.Belokopytov⁹, N.C.Benekos³³, A.C.Benvenuti⁵, C.Berat¹⁵, M.Berggren²⁴, D.Bertrand², M.Besancon⁴¹, M.Big⁴⁷, M.S.Bilenky¹⁷, M-A.Bizouard²⁰, D.Bloch¹⁰, H.M.Blom³², M.Bonesini²⁹, M.Boonekamp⁴¹, P.S.L.Booth²³, A.W.Borgland⁴, G.Borisov²⁰, C.Bosio⁴³, O.Botner⁵⁰, E.Boudinov³², B.Bouquet²⁰, C.Bourdarios²⁰, T.J.V.Bowcock²³, I.Boyko¹⁷, I.Bozovic¹², M.Bozzo¹⁴, M.Bracko⁴⁵, P.Branchini⁴⁰, R.A.Brenner⁵⁰, P.Bruckman⁹, J-M.Brunet⁸, L.Bugge³⁴, T.Buran³⁴, B.Buschbeck⁵², P.Buschmann⁵⁴, S.Cabrera⁵¹, M.Caccia²⁸, M.Calvi²⁹, T.Camporesi⁹, V.Canale³⁹, F.Carena⁹, L.Carroll²³, C.Caso¹⁴, M.V.Castillo Gimenez⁵¹, A.Cattai⁹, F.R.Cavallo⁵, V.Chabaud⁹, Ph.Charpentier⁹, P.Checchia³⁷, G.A.Chelkov¹⁷, R.Chierici⁴⁷, P.Chliapnikov^{9,44}, P.Chochula⁷, V.Chorowicz²⁶, J.Chudoba³¹, K.Cieslik¹⁹, P.Collins⁹, R.Contri¹⁴, E.Cortina⁵¹, G.Cosme²⁰, F.Cossutti⁹, H.B.Crawley¹, D.Crennell³⁸, S.Crepe¹⁵, G.Crosetti¹⁴, J.Cuevas Maestro³⁵, S.Czellar¹⁶, M.Davenport⁹, W.Da Silva²⁴, G.Della Ricca⁴⁸, P.Delpierre²⁷, N.Demaria⁹, A.De Angelis⁴⁸, W.De Boer¹⁸, C.De Clercq², B.De Lotto⁴⁸, A.De Min³⁷, L.De Paula⁴⁹, H.Dijkstra⁹, L.Di Ciaccio^{9,39}, J.Dolbeau⁸, K.Doroba⁵³, M.Dracos¹⁰, J.Drees⁵⁴, M.Dris³³, A.Duperrin²⁶, J-D.Durand⁹, G.Eigen⁴, T.Ekelo⁵⁰, G.Ekspong⁴⁶, M.Ellert⁵⁰, M.Elsing⁹, J-P.Engel¹⁰, M.Espirito Santo⁹, G.Fanourakis¹², D.Fassouliotis¹², J.Fayot²⁴, M.Feindt¹⁸, A.Ferrer⁵¹, E.Ferrer-Ribas²⁰, F.Ferro¹⁴, S.Fichet²⁴, A.Firestone¹, U.Flagmeyer⁵⁴, H.Foeth⁹, E.Fokitis³³, F.Fontanelli¹⁴, B.Franek³⁸, A.G.Frodesen⁴, R.Fruhwrith⁵², F.Fulda-Quenzer²⁰, J.Fuster⁵¹, A.Galloni²³, D.Gamba⁴⁷, S.Gamblin²⁰, M.Gandelman⁴⁹, C.Garcia⁵¹, C.Gaspar⁹, M.Gaspar⁴⁹, U.Gasparini³⁷, Ph.Gavillet⁹, E.N.Gaziz³³, D.Gel¹⁰, T.Geralis¹², L.Gerdyukov⁴⁴, N.Ghodbane²⁶, I.Gil⁵¹, F.Glege⁵⁴, R.Gokieli^{9,53}, B.Golob^{9,45}, G.Gomez-Ceballos⁴², P.Goncalves²², I.Gonzalez Caballero⁴², G.Gopal³⁸, L.Gorn¹, Yu.Gouz⁴⁴, V.Gracco¹⁴, J.Grahl¹, E.Graziani⁴⁰, P.Gris⁴¹, G.Grosdidier²⁰, K.Grzelak⁵³, J.Guy³⁸, C.Haag¹⁸, F.Hahn⁹, S.Hahn⁵⁴, S.Haider⁹, A.Hallgren⁵⁰, K.Hamacher⁵⁴, J.Hansen³⁴, F.J.Harris³⁶, V.Hedberg^{9,25}, S.Heising¹⁸, J.J.Hernandez⁵¹, P.Herquet², H.Herr⁹, T.L.Hessing³⁶, J.-M.Heuser⁵⁴, E.Higon⁵¹, S-O.Holmgren⁴⁶, P.J.Holt³⁶, S.Hoorelbeke², M.Houlden²³, J.Hrubic⁵², M.Huber¹⁸, K.Huet², G.J.Hughes²³, K.Hultqvist^{9,46}, J.N.Jackson²³, R.Jacobsson⁹, P.Jalocha¹⁹, R.Janik⁷, Ch.Jarlskog²⁵, G.Jarlskog²⁵, P.Jarry⁴¹, B.Jean-Marie²⁰, D.Jeans³⁶, E.K.Johansson⁴⁶, P.Jonsson²⁶, C.Joram⁹, P.Juillot¹⁰, L.Jungermann¹⁸, F.Kapusta²⁴, K.Karafasoulis¹², S.Katsanevas²⁶, E.C.Katsoufis³³, R.Keranen¹⁸, G.Kernel⁴⁵, B.P.Kersevan⁴⁵, Yu.Khokhlov⁴⁴, B.A.Khomenko¹⁷, N.N.Khovanski¹⁷, A.Kiiskinen¹⁶, B.King²³, A.Kinvig²³, N.J.Kjaer⁹, O.Klapp⁵⁴, H.Klein⁹, P.Kluit³², P.Kokkinias¹², V.Kostioukhine⁴⁴, C.Kourkoumelis³, O.Kouznetsov¹⁷, M.Krammer⁵², E.Kriznic⁴⁵, Z.Krumstein¹⁷, P.Kubinec⁷, J.Kurowska⁵³, K.Kurvinen¹⁶, J.W.Lamsa¹, D.W.Lane¹, V.Lapin⁴⁴, J-P.Laugier⁴¹, R.Lauhakangas¹⁶, G.Leder⁵², F.Ledroit¹⁵, V.Lefebure², L.Leinonen⁴⁶, A.Leisos¹², R.Leitner³¹, J.Lemonne², G.Lenzen⁵⁴, V.Lepeltier²⁰, T.Lesiak¹⁹, M.Lethuillier⁴¹, J.Libby³⁶, W.Liebig⁵⁴, D.Liko⁹, A.Lipniacka^{9,46}, I.Lippi³⁷, B.Loerstad²⁵, J.G.Loken³⁶, J.H.Lopes⁴⁹, J.M.Lopez⁴², R.Lopez-Fernandez¹⁵, D.Loukas¹², P.Lutz⁴¹, L.Lyons³⁶, J.MacNaughton⁵², J.R.Mahon⁶, A.Maio²², A.Malek⁵⁴, T.G.M.Malmgren⁴⁶, S.Maltezos³³, V.Malychev¹⁷, F.Mandl⁵², J.Marco⁴², R.Marco⁴², B.Marechal⁴⁹, M.Margoni³⁷, J-C.Marin⁹, C.Mariotti⁹, A.Markou¹², C.Martinez-Rivero²⁰, F.Martinez-Vidal⁵¹, S.Marti i Garcia⁹, J.Masik¹³, N.Mastroiannopoulos¹², F.Matorras⁴², C.Matteuzzi²⁹, G.Matthiae³⁹, F.Mazzucato³⁷, M.Mazzucato³⁷, M.Mc Cubbin²³, R.Mc Kay¹, R.Mc Nulty²³, G.Mc Pherson²³, C.Meroni²⁸, W.T.Meyer¹, E.Migliore⁹, L.Mirabito²⁶, W.A.Mitaroff⁵², U.Mjoernmark²⁵, T.Moa⁴⁶, M.Moch¹⁸, R.Moeller³⁰, K.Moenig^{9,11}, M.R.Monge¹⁴, D.Moraes⁴⁹, X.Moreau²⁴, P.Moretini¹⁴, G.Morton³⁶, U.Mueller⁵⁴, K.Muenich⁵⁴, M.Mulders³², C.Mulet-Marquis¹⁵, R.Muresan²⁵, W.J.Murray³⁸, B.Muryn¹⁹, G.Myatt³⁶, T.Myklebust³⁴, F.Naraghi¹⁵, M.Nassiakou¹², F.L.Navarria⁵, S.Navas⁵¹, K.Nawrocki⁵³, P.Negri²⁹, N.Neufeld⁹, R.Nicolaidou⁴¹, B.S.Nielsen³⁰, P.Niezurawski⁵³, M.Nikolenko^{10,17}, V.Nomokonov¹⁶, A.Nygren²⁵, V.Obraztsov⁴⁴, A.G.Olshevski¹⁷, A.Onofre²², R.Orava¹⁶, G.Orazi¹⁰, K.Osterberg¹⁶, A.Ouraou⁴¹, M.Paganoni²⁹, S.Paiano⁵, R.Pain²⁴, R.Paiva²², J.Palacios³⁶, H.Palka¹⁹, Th.D.Papadopoulou^{9,33}, L.Pape⁹, C.Parkes⁹, F.Parodi¹⁴, U.Parzefall²³, A.Passeri⁴⁰, O.Passon⁵⁴, T.Pavel²⁵, M.Pegoraro³⁷, L.Peralta²², M.Pernicka⁵², A.Perrotta⁵, C.Petridou⁴⁸, A.Petrolini¹⁴, H.T.Phillips³⁸, F.Pierre⁴¹, M.Pimenta²², E.Piotto²⁸, T.Podobnik⁴⁵, M.E.Pol⁶, G.Polok¹⁹, P.Poropat⁴⁸, V.Pozdniakov¹⁷, P.Privitera³⁹, N.Pukhaeva¹⁷, A.Pullia²⁹, D.Radojicic³⁶, S.Ragazzi²⁹, H.Rahmani³³, J.Rames¹³, P.N.Ratoff²¹, A.L.Read³⁴, P.Rebecchi⁹, N.G.Redaeli²⁹, M.Regler⁵², J.Rehn¹⁸, D.Reid³², R.Reinhardt⁵⁴, P.B.Renton³⁶, L.K.Resvanis³, F.Richard²⁰, J.Ridky¹³, G.Rinaudo⁴⁷, I.Ripp-Baudot¹⁰, O.Rohne³⁴, A.Romero⁴⁷, P.Ronchese³⁷, E.I.Rosenberg¹, P.Rosinsky⁷, P.Roudeau²⁰, T.Rovelli⁵, Ch.Royon⁴¹, V.Ruhmann-Kleider⁴¹, A.Ruiz⁴², H.Saarikko¹⁶, Y.Sacquin⁴¹, A.Sadovsky¹⁷, G.Sajot¹⁵, J.Salt⁵¹, D.Sampsonidis¹², M.Sannino¹⁴, Ph.Schwemling²⁴, B.Schwering⁵⁴, U.Schwickerath¹⁸, F.Scuri⁴⁸, P.Seager²¹, Y.Sedykh¹⁷, A.M.Segar³⁶, N.Seibert¹⁸, R.Sekulin³⁸, R.C.Shellard⁶, M.Siebel⁵⁴, L.Simard⁴¹, F.Simonetto³⁷, A.N.Sisakian¹⁷, G.Smadja²⁶, N.Smirnov⁴⁴, O.Smirnova²⁵, G.R.Smith³⁸, A.Sokolov⁴⁴, A.Sopczak¹⁸, R.Sosnowski⁵³, T.Spassov²², E.Spiriti⁴⁰, S.Squarcia¹⁴, C.Stanescu⁴⁰, S.Stanic⁴⁵, M.Stanitzki¹⁸, K.Stevenson³⁶, A.Stocchi²⁰, J.Strauss⁵², R.Strub¹⁰, B.Stugu⁴, M.Szczekowski⁵³, M.Szeptycka⁵³, T.Tabarelli²⁹, A.Taffard²³, F.Tegenfeldt⁵⁰, F.Terranova²⁹, J.Thomas³⁶, J.Timmermans³², N.Tinti⁵, L.G.Tkatchev¹⁷, M.Tobin²³, S.Todorova⁹, A.Tomaradze², B.Tome²², A.Tonazzo⁹, L.Tortora⁴⁰, P.Tortosa⁵¹, G.Transtromer²⁵, D.Treille⁹, G.Tristram⁸, M.Trochimczuk⁵³, C.Troncon²⁸, M-L.Turluer⁴¹,

I.A.Tyapkin¹⁷, P.Tyapkin²⁵, S.Tzamarias¹², O.Ullaland⁹, V.Uvarov⁴⁴, G.Valenti^{9,5}, E.Vallazza⁴⁸, C.Vander Velde², P.Van Dam³², W.Van den Boeck², W.K.Van Doninck², J.Van Eldik^{9,32}, A.Van Lysebetten², N.van Remortel², I.Van Vulpen³², G.Vegni²⁸, L.Ventura³⁷, W.Venus^{38,9}, F.Verbeure², P.Verdier²⁶, M.Verlato³⁷, L.S.Vertogradov¹⁷, V.Verzi²⁸, D.Vilanova⁴¹, L.Vitale⁴⁸, E.Vlasov⁴⁴, A.S.Vodopyanov¹⁷, G.Voulgaris³, V.Vrba¹³, H.Wahlen⁵⁴, C.Walck⁴⁶, A.J.Washbrook²³, C.Weiser⁹, D.Wicke⁵⁴, J.H.Wickens², G.R.Wilkinson³⁶, M.Winter¹⁰, M.Witek¹⁹, G.Wolf⁹, J.Yi¹, O.Yushchenko⁴⁴, A.Zalewska¹⁹, P.Zalewski⁵³, D.Zavrtanik⁴⁵, E.Zevgolatakos¹², N.I.Zimin^{17,25}, A.Zintchenko¹⁷, Ph.Zoller¹⁰, G.C.Zucchelli⁴⁶, G.Zumerle³⁷

¹Department of Physics and Astronomy, Iowa State University, Ames IA 50011-3160, USA

²Physics Department, Univ. Instelling Antwerpen, Universiteitsplein 1, B-2610 Antwerpen, Belgium and IIHE, ULB-VUB, Pleinlaan 2, B-1050 Brussels, Belgium

and Faculté des Sciences, Univ. de l'Etat Mons, Av. Maistriau 19, B-7000 Mons, Belgium

³Physics Laboratory, University of Athens, Solonos Str. 104, GR-10680 Athens, Greece

⁴Department of Physics, University of Bergen, Allégaten 55, NO-5007 Bergen, Norway

⁵Dipartimento di Fisica, Università di Bologna and INFN, Via Irnerio 46, IT-40126 Bologna, Italy

⁶Centro Brasileiro de Pesquisas Físicas, rua Xavier Sigaud 150, BR-22290 Rio de Janeiro, Brazil and Depto. de Física, Pont. Univ. Católica, C.P. 38071 BR-22453 Rio de Janeiro, Brazil

and Inst. de Física, Univ. Estadual do Rio de Janeiro, rua São Francisco Xavier 524, Rio de Janeiro, Brazil

⁷Comenius University, Faculty of Mathematics and Physics, Mlynska Dolina, SK-84215 Bratislava, Slovakia

⁸Collège de France, Lab. de Physique Corpusculaire, IN2P3-CNRS, FR-75231 Paris Cedex 05, France

⁹CERN, CH-1211 Geneva 23, Switzerland

¹⁰Institut de Recherches Subatomiques, IN2P3 - CNRS/ULP - BP20, FR-67037 Strasbourg Cedex, France

¹¹Now at DESY-Zeuthen, Platanenallee 6, D-15735 Zeuthen, Germany

¹²Institute of Nuclear Physics, N.C.S.R. Demokritos, P.O. Box 60228, GR-15310 Athens, Greece

¹³FZU, Inst. of Phys. of the C.A.S. High Energy Physics Division, Na Slovance 2, CZ-180 40, Praha 8, Czech Republic

¹⁴Dipartimento di Fisica, Università di Genova and INFN, Via Dodecaneso 33, IT-16146 Genova, Italy

¹⁵Institut des Sciences Nucléaires, IN2P3-CNRS, Université de Grenoble 1, FR-38026 Grenoble Cedex, France

¹⁶Helsinki Institute of Physics, HIP, P.O. Box 9, FI-00014 Helsinki, Finland

¹⁷Joint Institute for Nuclear Research, Dubna, Head Post Office, P.O. Box 79, RU-101 000 Moscow, Russian Federation

¹⁸Institut für Experimentelle Kernphysik, Universität Karlsruhe, Postfach 6980, DE-76128 Karlsruhe, Germany

¹⁹Institute of Nuclear Physics and University of Mining and Metallurgy, Ul. Kawiorów 26a, PL-30055 Krakow, Poland

²⁰Université de Paris-Sud, Lab. de l'Accélérateur Linéaire, IN2P3-CNRS, Bât. 200, FR-91405 Orsay Cedex, France

²¹School of Physics and Chemistry, University of Lancaster, Lancaster LA1 4YB, UK

²²LIP, IST, FCUL - Av. Elias Garcia, 14-1^o, PT-1000 Lisboa Codex, Portugal

²³Department of Physics, University of Liverpool, P.O. Box 147, Liverpool L69 3BX, UK

²⁴LPNHE, IN2P3-CNRS, Univ. Paris VI et VII, Tour 33 (RdC), 4 place Jussieu, FR-75252 Paris Cedex 05, France

²⁵Department of Physics, University of Lund, Sölvegatan 14, SE-223 63 Lund, Sweden

²⁶Université Claude Bernard de Lyon, IPNL, IN2P3-CNRS, FR-69622 Villeurbanne Cedex, France

²⁷Univ. d'Aix - Marseille II - CPP, IN2P3-CNRS, FR-13288 Marseille Cedex 09, France

²⁸Dipartimento di Fisica, Università di Milano and INFN-MILANO, Via Celoria 16, IT-20133 Milan, Italy

²⁹Dipartimento di Fisica, Univ. di Milano-Bicocca and INFN-MILANO, Piazza delle Scienze 2, IT-20126 Milan, Italy

³⁰Niels Bohr Institute, Blegdamsvej 17, DK-2100 Copenhagen Ø, Denmark

³¹IPNP of MFF, Charles Univ., Areal MFF, V Holesovickach 2, CZ-180 00, Praha 8, Czech Republic

³²NIKHEF, Postbus 41882, NL-1009 DB Amsterdam, The Netherlands

³³National Technical University, Physics Department, Zografou Campus, GR-15773 Athens, Greece

³⁴Physics Department, University of Oslo, Blindern, NO-1000 Oslo 3, Norway

³⁵Dpto. Física, Univ. Oviedo, Avda. Calvo Sotelo s/n, ES-33007 Oviedo, Spain

³⁶Department of Physics, University of Oxford, Keble Road, Oxford OX1 3RH, UK

³⁷Dipartimento di Fisica, Università di Padova and INFN, Via Marzolo 8, IT-35131 Padua, Italy

³⁸Rutherford Appleton Laboratory, Chilton, Didcot OX11 0QX, UK

³⁹Dipartimento di Fisica, Università di Roma II and INFN, Tor Vergata, IT-00173 Rome, Italy

⁴⁰Dipartimento di Fisica, Università di Roma III and INFN, Via della Vasca Navale 84, IT-00146 Rome, Italy

⁴¹DAPNIA/Service de Physique des Particules, CEA-Saclay, FR-91191 Gif-sur-Yvette Cedex, France

⁴²Instituto de Física de Cantabria (CSIC-UC), Avda. los Castros s/n, ES-39006 Santander, Spain

⁴³Dipartimento di Fisica, Università degli Studi di Roma La Sapienza, Piazzale Aldo Moro 2, IT-00185 Rome, Italy

⁴⁴Inst. for High Energy Physics, Serpukov P.O. Box 35, Protvino, (Moscow Region), Russian Federation

⁴⁵J. Stefan Institute, Jamova 39, SI-1000 Ljubljana, Slovenia and Laboratory for Astroparticle Physics,

Nova Gorica Polytechnic, Kostanjevska 16a, SI-5000 Nova Gorica, Slovenia,

and Department of Physics, University of Ljubljana, SI-1000 Ljubljana, Slovenia

⁴⁶Fysikum, Stockholm University, Box 6730, SE-113 85 Stockholm, Sweden

⁴⁷Dipartimento di Fisica Sperimentale, Università di Torino and INFN, Via P. Giuria 1, IT-10125 Turin, Italy

⁴⁸Dipartimento di Fisica, Università di Trieste and INFN, Via A. Valerio 2, IT-34127 Trieste, Italy

and Istituto di Fisica, Università di Udine, IT-33100 Udine, Italy

⁴⁹Univ. Federal do Rio de Janeiro, C.P. 68528 Cidade Univ., Ilha do Fundão BR-21945-970 Rio de Janeiro, Brazil

⁵⁰Department of Radiation Sciences, University of Uppsala, P.O. Box 535, SE-751 21 Uppsala, Sweden

⁵¹IFIC, Valencia-CSIC, and D.F.A.M.N., U. de Valencia, Avda. Dr. Moliner 50, ES-46100 Burjassot (Valencia), Spain

⁵²Institut für Hochenergiephysik, Österr. Akad. d. Wissensch., Nikolsdorfergasse 18, AT-1050 Vienna, Austria

⁵³Inst. Nuclear Studies and University of Warsaw, Ul. Hoza 69, PL-00681 Warsaw, Poland

⁵⁴Fachbereich Physik, University of Wuppertal, Postfach 100 127, DE-42097 Wuppertal, Germany

1 Introduction

This paper reports on a search for scalar partners of quarks (squarks) in data taken by DELPHI in 1997 and 1998 at centre-of-mass energies (\sqrt{s}) of 183 GeV and 189 GeV. Mass limits for these particles have already been published based on data taken at LEP2 [1], [2].

Scalar partners of right- and left-handed fermions are predicted by supersymmetric models and, in particular, by the minimal supersymmetric extension of the standard model (MSSM) [3]. They could be produced pairwise via e^+e^- annihilation into Z^0/γ . Large Yukawa coupling running for the diagonal elements and important off-diagonal terms make the partners of heavy fermions as the most probable candidates for the charged lightest supersymmetric particle. As a consequence their lighter states are candidates for the lightest charged supersymmetric particle.

Throughout this paper conservation of R-parity is assumed, which implies that the lightest supersymmetric particle (LSP) is stable. The LSP is assumed to be the lightest neutralino which interacts only weakly with matter, such that events will be characterised by missing momentum and energy.

In a large fraction of the MSSM parameter space sfermions are predicted to decay dominantly into the corresponding fermion and the lightest neutralino. Consequently in the search for sbottom particles only the decay into $b + \tilde{\chi}_1^0$ was considered. For the stop squark, the equivalent decay into $t + \tilde{\chi}_1^0$ is kinematically not allowed at LEP, and the decay of a stop into a bottom quark and a chargino is disfavoured in view of existing limits on the chargino mass [4]. The dominant two-body decay channel is thus the one into a charm quark and a neutralino.

2 Detector description

The DELPHI detector and its performance have been described in detail elsewhere [5,6]; only those components relevant for the present analyses are discussed here. Charged particle tracks are reconstructed in the 1.2 T solenoidal magnetic field by a system of cylindrical tracking chambers. These are the Vertex Detector (VD), the Inner Detector (ID), the Time Projection Chamber (TPC) and the Outer Detector (OD). In addition, two planes of drift chambers aligned perpendicular to the beam axis (Forward Chambers A and B) track particles in the forward and backward directions, covering polar angles $11^\circ < \theta < 33^\circ$ and $147^\circ < \theta < 169^\circ$ with respect to the beam (z) direction.

The VD consists of three cylindrical layers of silicon detectors, at radii 6.3 cm, 9.0 cm and 11.0 cm. All three layers measure coordinates in the plane transverse to the beam. The inner (6.3 cm) and the outer (11.0 cm) layers contain double-sided detectors to also measure z coordinates. The VD covers polar angles from 24° to 156° . The ID consists of a cylindrical drift chamber (inner radius 12 cm and outer radius 22 cm) covering polar angles between 15° and 165° . The TPC, the principal tracking device of DELPHI, consists of a cylinder of 30 cm inner radius, 122 cm outer radius and has a length of 2.7 m. Each end-plate has been divided into 6 sectors, with 192 sense wires used for the dE/dx measurement and 16 circular pad rows used for 3 dimensional space-point reconstruction. The OD consists of 5 layers of drift cells at radii between 192 cm and 208 cm, covering polar angles between 43° and 137° .

The average momentum resolution for the charged particles in hadronic final states is in the range $\Delta p/p^2 \simeq 0.001$ to $0.01(\text{GeV}/c)^{-1}$, depending on which detectors are used in the track fit [6].

The electromagnetic calorimeters consist of the High density Projection Chamber (HPC) covering the barrel region of $40^\circ < \theta < 140^\circ$, the Forward ElectroMagnetic Calorimeter (FEMC) covering $11^\circ < \theta < 36^\circ$ and $144^\circ < \theta < 169^\circ$, and the STIC, a Scintillator Tile Calorimeter which extends the coverage down to 1.66° from the beam axis in both directions. The 40° taggers are made of single layer scintillator-lead counters used to veto electromagnetic particles that may be not measured in the region between the HPC and FEMC. The efficiency to register a photon with energy above 5 GeV at polar angles between 20° and 160° , measured with the LEP1 data, is greater than 99% [6]. The hadron calorimeter (HCAL) covers 98% of the solid angle. Muons with momenta above 2 GeV/c penetrate the HCAL and are recorded in a set of Muon Drift Chambers.

Decays of b-quarks are tagged using a probabilistic method based on the impact parameters of tracks with respect to the main vertex. \mathcal{P}_E^+ stands for the corresponding probability estimator for tracks with positive impact parameters, the sign of the impact parameter being defined by the jet direction. The combined probability estimator \mathcal{P}_{comb} includes in addition contributions from properties of reconstructed secondary vertices [7].

3 Data samples and event generators

Data were taken during the 1997 and 1998 LEP runs at mean centre-of-mass energies of 183 GeV and 189 GeV, corresponding to integrated luminosities of 54 pb^{-1} and 158 pb^{-1} .

Simulated events were generated with several programs in order to evaluate the signal efficiency and the background contamination. All the models used JETSET 7.4 [8] for quark fragmentation with parameters tuned to represent DELPHI data [9].

Stop events were generated according to the expected differential cross-sections, using the BASES and SPRING program packages [10]. Special care was taken in the modelling of the stop hadronisation [11]. Sbottom events were generated with the SUSYGEN program [12]. The background processes $e^+e^- \rightarrow q\bar{q}(n\gamma)$ and processes leading to four-fermion final states, $(Z^0/\gamma)^*(Z^0/\gamma)^*$, W^+W^- , $W\nu_e$, and $Z^0e^+e^-$ were generated using PYTHIA [8]. At the generator level, the cut on the invariant mass of the virtual $(Z^0/\gamma)^*$ in the $(Z^0/\gamma)^*(Z^0/\gamma)^*$ process was set at $2 \text{ GeV}/c^2$, in order to be able to estimate the background from low mass $f\bar{f}$ pairs. The calculation of the four-fermion background was cross-checked using the program EXCALIBUR [13], which consistently takes into account all amplitudes leading to a given four-fermion final state. The version of EXCALIBUR used does not, however, include the transverse momentum of initial state radiation. Two-photon interactions leading to hadronic final states were simulated using TWOGAM [14] and BDKRC [15] for the Quark Parton Model contribution. Leptonic final states with muons and taus were also modelled with BDKRC. BDK [15] was used for final states with electrons only.

Generated signal and background events were passed through detailed detector response simulation [6] and processed with the same reconstruction and analysis programs as the real data. The number of background events simulated is mostly several times larger than the number expected in the real data.

4 Event selection

In this section the selection to search for stop and sbottom in the decay modes $c\tilde{\chi}_1^0$ and $b\tilde{\chi}_1^0$, respectively, is presented. In both cases the experimental signatures consist of events with two jets and missing momentum. Since event parameters, such as visible

energy, greatly depend on the mass difference ΔM between the squark and the LSP, optimised selection procedures are used for the degenerate ($\Delta M \leq 10 \text{ GeV}/c^2$), and the non-degenerate ($\Delta M > 10 \text{ GeV}/c^2$) mass case. The main differences between stop and sbottom events arise from the hadronisation, which occurs either before (\tilde{t}) or after (\tilde{b}) the decay of the scalar quark (in a large fraction of the MSSM parameter space the width of the sbottom decay into $b + \tilde{\chi}_1^0$ is greater than the typical QCD scale so that the sbottom does not hadronize before it decays). These differences are visible in particular in the degenerate mass case. Consequently different selections are used for the stop and sbottom analyses in the degenerate mass case whereas the selections are identical in the non-degenerate mass case.

In a first step particles are selected and clustered into jets using the Durham algorithm [16] with $y_{cut} = 0.08$. Reconstructed charged particles are required to have momenta above $100 \text{ MeV}/c$ and impact parameters to the measured interaction point below 4 cm in the transverse plane and below 10 cm in the beam direction. Clusters in the calorimeters are interpreted as neutral particles if they are not associated to charged particles, and if their energy exceeds 100 MeV.

In the second step of the analysis, hadronic events are selected. Only two-jet events are accepted. The following requirements are optimised separately for the two ΔM regions:

Non-degenerate mass case: For both the stop and sbottom analyses hadronic events are selected by requiring at least eight charged particles, a total transverse energy¹ greater than 15 GeV and a transverse energy of the most energetic jet greater than 10 GeV. These three cuts are aimed at reducing the background coming from two-photon processes. Forward Bhabha scattering is suppressed by requiring that the total energy in the FEMC is lower than 25 GeV. $Z^0(\gamma)$ processes with a detected photon are reduced by requiring that the total energy in the HPC is lower than 40 GeV. Finally, at $\sqrt{s} = 183 \text{ GeV}$, the requirement for substantial missing energy is fulfilled by demanding that the quantity $\sqrt{s'}$ is lower than 170 GeV. The quantity $\sqrt{s'}$ is the effective centre-of-mass energy after photons radiation from the incoming e^+e^- beams. At $\sqrt{s} = 189 \text{ GeV}$, this requirement is replaced by the requirement that the polar angles of the two jets are between 20° and 160° .

Degenerate mass case: To select hadronic events in the stop analysis the number of charged particles is required to be greater than five, the total charged energy has to be lower than $0.3\sqrt{s}$ (in order to select events with missing energy) and the polar angle of the total missing momentum has to be between 15° and 165° , in order to reduce the background from radiative return events. The total energy in the FEMC and HPC has to be lower than 10 GeV and 40 GeV, respectively. The reduction of two-photon processes is ensured by requiring that the total transverse energy is greater than 5 GeV and that the quantity $p_{tt} = \sqrt{p_{tt1}^2 + p_{tt2}^2}$ is greater than $5 \text{ GeV}/c$, where p_{tti} is the transverse momentum of jet i with respect to the thrust axis projected onto the plane transverse to the beam axis. Finally, the most energetic charged particle is required to have a polar angle between 30° and 150° and a momentum greater than $2 \text{ GeV}/c$. Similarly the polar angle of the most energetic neutral particle is required to be between 20° and 160° . At $\sqrt{s} = 183 \text{ GeV}$, the sbottom selection at this step is similar to the stop analysis described above except for the requirement on p_{tt} which is replaced by requiring the ratio p_{tt}/E_{tot} to be greater than 50% where E_{tot} is the total energy of the event.

¹The transverse energy E_t of a particle is defined as $E_t = \sqrt{E_x^2 + E_y^2}$ where E_x and E_y respectively are $E \cos \phi \sin \theta$ and $E \sin \phi \sin \theta$. The angles ϕ and θ are respectively the azimuthal and polar angle of the particle.

At $\sqrt{s} = 189$ GeV, the sbottom selection at this step is simplified by removing the above requirement on p_{tt}/E_{tot} .

After this second step and for both the non-degenerate and the degenerate mass cases, agreement between data and expectations from the Monte Carlo simulation describing standard model processes is found to be good as can be seen from Figures 1a-c showing the visible mass, the charged multiplicity and the fraction of the energy for polar angles between 30° and 150° at $\sqrt{s} = 189$ GeV. Figures 2a-c show the total energy, the transverse energy and the charged multiplicity of the leading jet, for the degenerate mass case of the stop analysis at $\sqrt{s} = 189$ GeV. Figures 3a-c show the visible mass, the missing transverse energy and the total multiplicity for the degenerate mass case of the sbottom analysis at $\sqrt{s} = 189$ GeV.

In a third step discriminating linear functions [17] are used in order to achieve optimum rejection power. They have been determined in the following way:

Non-degenerate mass case: In this case, the same functions have been used both for the stop and the sbottom analysis. A first discriminating linear function has been determined using training samples of signal and $Z^0(\gamma)$ background processes. For the training of a second discriminating linear function, signal and WW background event samples have been used. In the non-degenerate mass case, these two sources of background processes are found to be dominant after the first and second step of the event selection.

Degenerate mass case: Here the main source of background remaining after the first and second step of the event selection is found to be $\gamma\gamma$ events. Different functions have been determined for the stop and sbottom analyses using training samples of signal and two-photon events.

Figure 1d shows the discriminating function against the $Z^0\gamma$ background for the non-degenerate mass case at $\sqrt{s} = 189$ GeV, Figure 2d and 3d show the discriminating functions for the degenerate mass domains of the stop and sbottom analyses at $\sqrt{s} = 189$ GeV. For these degenerate and non-degenerate mass cases, fair agreements between data and expectations from Monte Carlo describing standard model processes are found. The data and Monte Carlo small disagreement of the discriminating function for the degenerate mass cases shown in Figure 2d is restricted to the negative values of this function which correspond to the region of the bulk of the expectations from Monte Carlo describing standard model processes in particular two-photon interactions leading to hadronic final states which are known to be difficult to modelize. This region does not correspond to the squark signal region. As shown by the hatched areas of Figure 2d, the positive values of this discriminating function correspond to the squark signal region and in this region the agreement between data and expectations from Monte Carlo describing standard model processes is very good.

The final background reduction is performed by sequential cuts. In the non-degenerate mass case, one set of cuts is used to select both stop and sbottom events. It is shown, together with the number of events retained in data and background simulation, in Tables 1 and 2.

In the degenerate mass case two different selections are used for stop and sbottom. These are shown in Table 3 for the stop analysis at $\sqrt{s} = 183$ GeV and $\sqrt{s} = 189$ GeV and in Tables 4 and 5 for the sbottom analysis at $\sqrt{s} = 183$ GeV and $\sqrt{s} = 189$ GeV respectively.

5 Results

The number of candidates found and the expected background levels are shown in Table 6 and Table 7. There are candidates in common in the stop and sbottom analyses. The total background is given assuming a //or// between the degenerate mass case and the non-degenerate mass case for the stop and sbottom analyses. One candidate event from the non-degenerate mass case analysis is shown in Figure 4. The efficiencies of the stop and sbottom signal selection are summarised in Figure 5. They have been evaluated using 35 simulated samples at different points in the $(M_{\tilde{q}}, M_{\tilde{\chi}_1^0})$ plane, for squark masses between 50 and 90 GeV/c^2 and neutralino masses between 0 and 85 GeV/c^2 .

No evidence for stop or sbottom production has been found in the two-body decay channels. Figure 6 and Figure 7 show the $(M_{\tilde{q}}, M_{\tilde{\chi}_1^0})$ regions excluded at 95% confidence level by the search for $\tilde{t} \rightarrow c\tilde{\chi}_1^0$ and $\tilde{b} \rightarrow b\tilde{\chi}_1^0$ decays, with the 100% branching ratio assumption, both for purely left-handed states (with maximum cross-section) and the states with minimum cross-section. We have also used the results (efficiencies, number of candidates and expected background) of the analyses of the data at 130 - 172 GeV [1] in order to derive these exclusion regions.

In order to estimate systematic errors coming from detector effects and modelling, the differences of the mean values of the observables used for the above analyses (sequential cuts steps and discriminating linear analyses steps) between real data and simulation are calculated at the level of the first step of the selection described in section 4. The difference δ for the mean value of the observable X between real data and simulation is used in order to shift X according to $X + \delta$ and $X - \delta$. The analyses described in section 4 then use the shifted observables and the differences in efficiencies and expected background with respect to efficiencies and expected background obtained with the unshifted observables are taken as systematic errors. The relative systematic errors for efficiencies are 10% in the non-degenerate mass case and 15% in the degenerate mass case. The systematic errors for the expected background are given in Table 6 and Table 7.

Systematic errors on efficiencies coming from the modelling of the hadronization of the stop are estimated by switching off the hadronization of the stop. The relative systematic errors for efficiencies are 2% in the non degenerate mass case and 8% in the degenerate mass case.

6 Conclusions

In data samples of 54 pb^{-1} and 158 pb^{-1} collected by the DELPHI detector at centre-of-mass energies of 183 GeV and 189 GeV searches are performed for events with acoplanar jet pairs. The results are combined with those already obtained at centre-of-mass energies between 130–172 GeV .

At 183 GeV, the search for stop and sbottom quarks, decaying into $c\tilde{\chi}_1^0$ and $b\tilde{\chi}_1^0$, respectively, gives in total 3 candidates (some candidates are in common in the stop and sbottom analyses) well compatible with the expected background of 3.4 ± 0.5 .

At 189 GeV, the search for stop and sbottom quarks, decaying into $c\tilde{\chi}_1^0$ and $b\tilde{\chi}_1^0$, respectively, gives in total 9 candidates (some are candidates are also in common in the stop and sbottom analyses) well compatible with the expected background of 11.6 ± 1.4 .

For the stop, a mass limit of 79 GeV/c^2 is obtained for the state with minimal cross-section, if the mass difference between the squark and the LSP is above 15 GeV/c^2 . A mass limit of 62 GeV/c^2 is obtained for the sbottom quark under the same condition.

In the case of maximum cross-section, these numbers are $84 \text{ GeV}/c^2$ for the stop and $87 \text{ GeV}/c^2$ for the sbottom.

Acknowledgements

We are greatly indebted to our technical collaborators, to the members of the CERN-SL Division for the excellent performance of the LEP collider, and to the funding agencies for their support in building and operating the DELPHI detector.

We acknowledge in particular the support of

Austrian Federal Ministry of Science and Traffic, GZ 616.364/2-III/2a/98,

FNRS-FWO, Belgium,

FINEP, CNPq, CAPES, FUJB and FAPERJ, Brazil,

Czech Ministry of Industry and Trade, GA CR 202/96/0450 and GA AVCR A1010521,

Danish Natural Research Council,

Commission of the European Communities (DG XII),

Direction des Sciences de la Matière, CEA, France,

Bundesministerium für Bildung, Wissenschaft, Forschung und Technologie, Germany,

General Secretariat for Research and Technology, Greece,

National Science Foundation (NWO) and Foundation for Research on Matter (FOM),

The Netherlands,

Norwegian Research Council,

State Committee for Scientific Research, Poland, 2P03B06015, 2P03B1116 and

SPUB/P03/178/98,

JNICT-Junta Nacional de Investigação Científica e Tecnológica, Portugal,

Vedecka grantova agentura MS SR, Slovakia, Nr. 95/5195/134,

Ministry of Science and Technology of the Republic of Slovenia,

CICYT, Spain, AEN96-1661 and AEN96-1681,

The Swedish Natural Science Research Council,

Particle Physics and Astronomy Research Council, UK,

Department of Energy, USA, DE-FG02-94ER40817.

References

- [1] DELPHI Collaboration: P. Abreu *et al.*, E. Phys. J. **C6** (1999) 385.
- [2] ALEPH Collaboration: R. Barate *et al.*, Phys. Lett. **B434** (1998) 189;
ALEPH Collaboration: R. Barate *et al.*, Phys. Lett. **B469** (1999) 303;
ALEPH Collaboration: R. Barate *et al.*, CERN-EP/2000-85;
L3 Collaboration, M. Acciari *et al.*, Phys. Lett. **B471** (1999) 308;
OPAL Collaboration: K. Ackerstaff *et al.*, Phys. Lett. **B396** (1997) 301;
OPAL Collaboration: K. Ackerstaff *et al.*, Z. Phys. **C75** (1997) 409;
OPAL Collaboration: G. Abbiendi *et al.*, Phys. Lett. **B456** (1999) 95.
- [3] P. Fayet and S. Ferrara, Phys. Rep. **32** (1977) 249;
H.P. Nilles, Phys. Rep. **110** (1984) 1;
H.E. Haber and G. L.Kane, Phys. Rep. **117** (1985) 75.
- [4] ALEPH Collaboration: R. Barate *et al.*, E. Phys. J. **C2** (1998) 417;
ALEPH Collaboration: R. Barate *et al.*, E. Phys. J. **C11** (1999) 193;
DELPHI Collaboration: P. Abreu *et al.*, E. Phys. J. **C1** (1998) 1;
L3 Collaboration: M. Acciarri *et al.*, Phys. Lett. **B472** (2000) 420;
OPAL Collaboration: K. Ackerstaff *et al.*, E. Phys. J. **C2** (1998) 213;
OPAL Collaboration: K. Ackerstaff *et al.*, E. Phys. J. **C14** (2000) 187.
- [5] DELPHI Collaboration: P. Aarnio *et al.*, Nucl. Instr. and Meth. **A303** (1991) 233.
- [6] DELPHI Collaboration: P. Abreu *et al.*, Nucl. Instr. and Meth. **A378** (1996) 57.
- [7] DELPHI Collaboration: P. Abreu *et al.*, Z. Phys. **C70** (1996) 531;
DELPHI Collaboration: P. Abreu *et al.*, E. Phys. J. **C10** (1999) 415.
- [8] T. Sjöstrand, Comp. Phys. Comm. **82** (1994) 74.
- [9] DELPHI Collaboration: P. Abreu *et al.*, Z. Phys. **C73** (1996) 11.
- [10] S. Kawabata, Comp. Phys. Comm. **41** (1986) 127.
- [11] W. Beenakker, R. Hopker, M. Spira, and P.M. Zerwas, Phys. Lett. **B349** (1995) 463.
- [12] S.Katsanevas and P.Morawitz, Comp. Phys. Comm. **112** (1998) 227.
- [13] F.A. Berends, R. Pittau, R. Kleiss, Comp. Phys. Comm. **85** (1995) 437.
- [14] T.Alderweird *et al.*, CERN-OPEN-2000-141
- [15] F.A. Berends, P.H. Daverveldt, R. Kleiss, Monte Carlo Simulation of Two-Photon Processes, Comp. Phys. Comm. **40** (1986) 271.
- [16] S. Catani, Yu.L. Dokshitzer, M. Olson, G. Turnock and B.R. Webber, Phys. Lett. **B269** (1991) 432.
- [17] R.A. Fisher, *The use of multiple measurements in taxonomic problems*, Annals of Eugenics, **7** (1936).
- [18] OPAL Collaboration: R. Akers *et al.*, Phys. Lett. **B337** (1994) 207.
- [19] CDF Collaboration: *Search for Scalar Top and Scalar Bottom Quarks in $p\bar{p}$ collisions at $\sqrt{s} = 1.8$ TeV*, hep-ex/9910049, submitted to Phys.Rev.Lett.

Selection	\tilde{t} and \tilde{b} : $\Delta M > 10 \text{ GeV}/c^2$ $\sqrt{s}=183 \text{ GeV}$	
	Data ₁₈₃	MC ₁₈₃
1 st and 2 nd step	2871	2682 ± 14
3 rd step (DLA1) > 0.9	98	100 ± 4
3 rd step (DLA2) $> 0.$	27	28 ± 3
$P_{T_{miss}} \geq 12 \text{ GeV}/c$	21	18 ± 2
$E_{jet1} \leq 60 \text{ GeV}$ $E_{emjet1}/E_{jet1} \leq 0.6$ $E_{emjet2}/E_{jet2} \leq 0.6$	7	4.4 ± 0.3
$20^\circ \leq \theta_{jets} \leq 160^\circ$	4	3.7 ± 0.3
$P_{iso} \leq 20 \text{ GeV}/c$	3	2.9 ± 0.3
$ \cos\theta_{thrust} \leq 0.9$	2	2.3 ± 0.3
$E_{T_{charged}}^{jet2} \geq 2 \text{ GeV}$	1	2.2 ± 0.3
Visible mass $\leq 70 \text{ GeV}/c^2$	1	1.8 ± 0.2
$< E_{charged} > \leq 4 \text{ GeV}$	1	1.4 ± 0.2

Table 1: Fourth step of the event selection for two-body decays of stop and sbottom in the non-degenerate mass case at $\sqrt{s} = 183 \text{ GeV}$. Data₁₈₃ and MC₁₈₃ indicate data and Monte Carlo at $\sqrt{s} = 183 \text{ GeV}$. DLA1 and DLA2 denote the first and second discriminating linear analysis as explained in the text. $P_{T_{miss}}$ stands for the total missing momentum, E_{jet1} (E_{jet2}) denotes the energy of the (next to) leading jet, E_{emjet1} (E_{emjet2}) denotes the total electromagnetic energy of the (next to) leading jet, θ_{jets} are the polar angles of the jets, P_{iso} is the momentum of the most isolated charged particle, θ_{thrust} denotes the polar angle of the thrust axis and $E_{T_{charged}}^{jet2}$ is the total transverse energy of the next to leading jet taking into account charged particles only. ΔM represents the mass difference between the squark and the LSP. The case $\Delta M > 10 \text{ GeV}/c^2$ corresponds to the non-degenerate mass case. The errors on the Monte Carlo are statistical only.

Selection	\tilde{t} and \tilde{b} : $\Delta M > 10 \text{ GeV}/c^2$ $\sqrt{s}=189 \text{ GeV}$	
	Data ₁₈₉	MC ₁₈₉
1 st and 2 nd step	6507	6659 \pm 12
3 rd step (DLA1) > 0.3	130	125 \pm 3
3 rd step (DLA2) > 0.4	22	24 \pm 2
$R_{30} > 0.80$	15	12.9 \pm 1.1
$R_{20} > 0.95$	12	11 \pm 0.9
$P^{leading} < 25 \text{ GeV}/c$	7	7.6 \pm 0.9
$E_{em2}/E(jet2) \leq 0.2$	5	7 \pm 0.9
$\mathcal{P}_{comb} \geq -1$ for \tilde{b} only	2	2.2 \pm 0.4

Table 2: Fourth step of the event selection for two-body decays of stop and sbottom in the non-degenerate mass case at $\sqrt{s} = 189 \text{ GeV}$. Data₁₈₉ and MC₁₈₉ indicate data and Monte Carlo at $\sqrt{s} = 189 \text{ GeV}$. DLA1 and DLA2 denote the first and second discriminating linear analysis as explained in the text. R_{30} (R_{20}) denotes the fraction of the total energy out of the cones of 30° and 150° (20° and 160°) centered on the beam axis. $P^{leading}$ denotes the momentum of the leading particle; E_{em2} denotes the total electromagnetic energy of the next to leading jet. \mathcal{P}_{comb} is a b-tagging probability as explained in the text. ΔM represents the mass difference between the squark and the LSP. The case $\Delta M > 10 \text{ GeV}/c^2$ corresponds to the non-degenerate mass case. The errors on the Monte Carlo are statistical only.

Selection	\tilde{t} : $\Delta M \leq 10 \text{ GeV}/c^2$			
	Data ₁₈₃	MC ₁₈₃	Data ₁₈₉	MC ₁₈₉
1 st and 2 nd step	575	528 \pm 7	1613	1567 \pm 45
3 rd step (DLA) > 0.3	44	45 \pm 2	139	134 \pm 10
oblateness ≥ 0.1	40	38 \pm 2	115	106 \pm 5
$R_{30} \geq 0.9$	24	25 \pm 1	76	79 \pm 4
$R_{20} \geq 0.985$	20	22 \pm 1	65	68 \pm 4
$P_{tt} \leq 30 \text{ GeV}/c$	8	13 \pm 1	29	40 \pm 4
acoplanarity _{thrust} $\geq 20^\circ$	1	2.6 \pm 0.5	8	8.1 \pm 1.6
cos(acoplanarity) ≥ -0.85	1	0.98 \pm 0.27	3	3.3 \pm 0.8

Table 3: Fourth step of the event selection for two-body decays of stop squarks in the degenerate mass case at $\sqrt{s} = 183 \text{ GeV}$ and $\sqrt{s} = 189 \text{ GeV}$. Data₁₈₃ and MC₁₈₃ (Data₁₈₉ and MC₁₈₉) indicate data and Monte Carlo at $\sqrt{s} = 183 \text{ GeV}$ ($\sqrt{s} = 189 \text{ GeV}$). R_{30} (R_{20}) denotes the fraction of the total energy out of the cones of 30° and 150° (20° and 160°) centered on the beam axis and acoplanarity_{thrust} the acoplanarity angle with respect to the thrust axis. For the other variables see the text as well as in Tables ??, ??, 1 and 2. DLA stands for discriminating linear analysis. ΔM represents the mass difference between the squark and the LSP. The case $\Delta M \leq 10 \text{ GeV}/c^2$ corresponds to the degenerate mass case. The errors on the Monte Carlo are statistical only.

Selection	\tilde{b} : $\Delta M \leq 10 \text{ GeV}/c^2$	
	Data ₁₈₃	MC ₁₈₃
1 st and 2 nd step	747	629 \pm 8
3 rd step (DLA) > 0.7	70	52 \pm 2
$E_{tot} \leq 40 \text{ GeV}$	42	34 \pm 2
$E_{T_{charged}}^{jet1} \geq 2 \text{ GeV}$	32	27 \pm 2
$20^\circ \leq \theta_{jets} \leq 160^\circ$	26	25 \pm 2
$E_T^{jet1} \geq 5 \text{ GeV}$	10	14 \pm 1
acoplanarity _{thrust} $\geq 20^\circ$	1	3 \pm 0.6
$E_{T_{charged}}^{jet2} \geq 1 \text{ GeV}$	1	2.5 \pm 0.5
$E_{T_{charged}}^{jet2} \geq 2 \text{ GeV}$	1	1.6 \pm 0.4
oblateness ≤ 0.36	1	1.1 \pm 0.3

Table 4: Fourth step of the event selection for two-body sbottom decays in the degenerate mass case at $\sqrt{s} = 183 \text{ GeV}$. Data₁₈₃ and MC₁₈₃ indicate data and Monte Carlo at $\sqrt{s} = 183 \text{ GeV}$. The variables are explained in the caption of Tables ??, ??, 1, 2 and 3. DLA stands for discriminating linear analysis. ΔM represents the mass difference between the squark and the LSP. The case $\Delta M \leq 10 \text{ GeV}/c^2$ corresponds to the degenerate mass case. The errors on the Monte Carlo are statistical only.

Selection	\tilde{b} : $\Delta M \leq 10 \text{ GeV}/c^2$	
	Data ₁₈₉	MC ₁₈₉
1 st and 2 nd step	5307	5644 \pm 106
3 rd step (DLA) > 0	19	26 \pm 7
$R_{20} \geq 0.98$	14	24 \pm 3
$R_{20} \times P_T^{miss} \geq 1 \text{ GeV}/c$	12	16 \pm 3
$P_{tt} \geq 4 \text{ GeV}/c$	7	9.7 \pm 2
$\cos(\text{acoplanarity}) \geq -0.98$	3	3.5 \pm 1
$\mathcal{P}_{comb} \geq -1$	1	2.3 \pm 0.8

Table 5: Fourth step of the event selection for two-body sbottom decays in the degenerate mass case at $\sqrt{s} = 189 \text{ GeV}$. Data₁₈₉ and MC₁₈₉ indicate data and Monte Carlo at $\sqrt{s} = 189 \text{ GeV}$. The variables are explained in the caption of Tables ??, ??, 1, 2 and 3. DLA stands for discriminating linear analysis. ΔM represents the mass difference between the squark and the LSP. The case $\Delta M \leq 10 \text{ GeV}/c^2$ corresponds to the degenerate mass case. The errors on the Monte Carlo are statistical only.

Squark	Data ₁₈₃	MC ₁₈₃
\tilde{t}	2	$2.4 \pm 0.3(\text{stat})_{-0.2}^{+0.2}(\text{syst})$
\tilde{b}	2	$2.6 \pm 0.4(\text{stat})_{-0.2}^{+0.3}(\text{syst})$

Table 6: Number of candidates and expected background in the search for two-body decays of stop and sbottom when performing the *//or//* of the analyses in the degenerate and non-degenerate mass case at $\sqrt{s} = 183$ GeV. Data₁₈₃ and MC₁₈₃ indicate data and Monte Carlo at $\sqrt{s} = 183$ GeV. There are candidates in common in the stop and sbottom analyses.

Squark	Data ₁₈₉	MC ₁₈₉
\tilde{t}	8	$9.3 \pm 1.2(\text{stat})_{-0.6}^{+0.9}(\text{syst})$
\tilde{b}	3	$4.4 \pm 0.9(\text{stat})_{-0.3}^{+0.6}(\text{syst})$

Table 7: Number of candidates and expected background in the search for two-body decays of stop and sbottom when performing the *//or//* of the analyses in the degenerate and non-degenerate mass case at $\sqrt{s} = 189$ GeV. Data₁₈₉ and MC₁₈₉ indicate data and Monte Carlo at $\sqrt{s} = 189$ GeV. There are candidates in common in the stop and sbottom analyses.

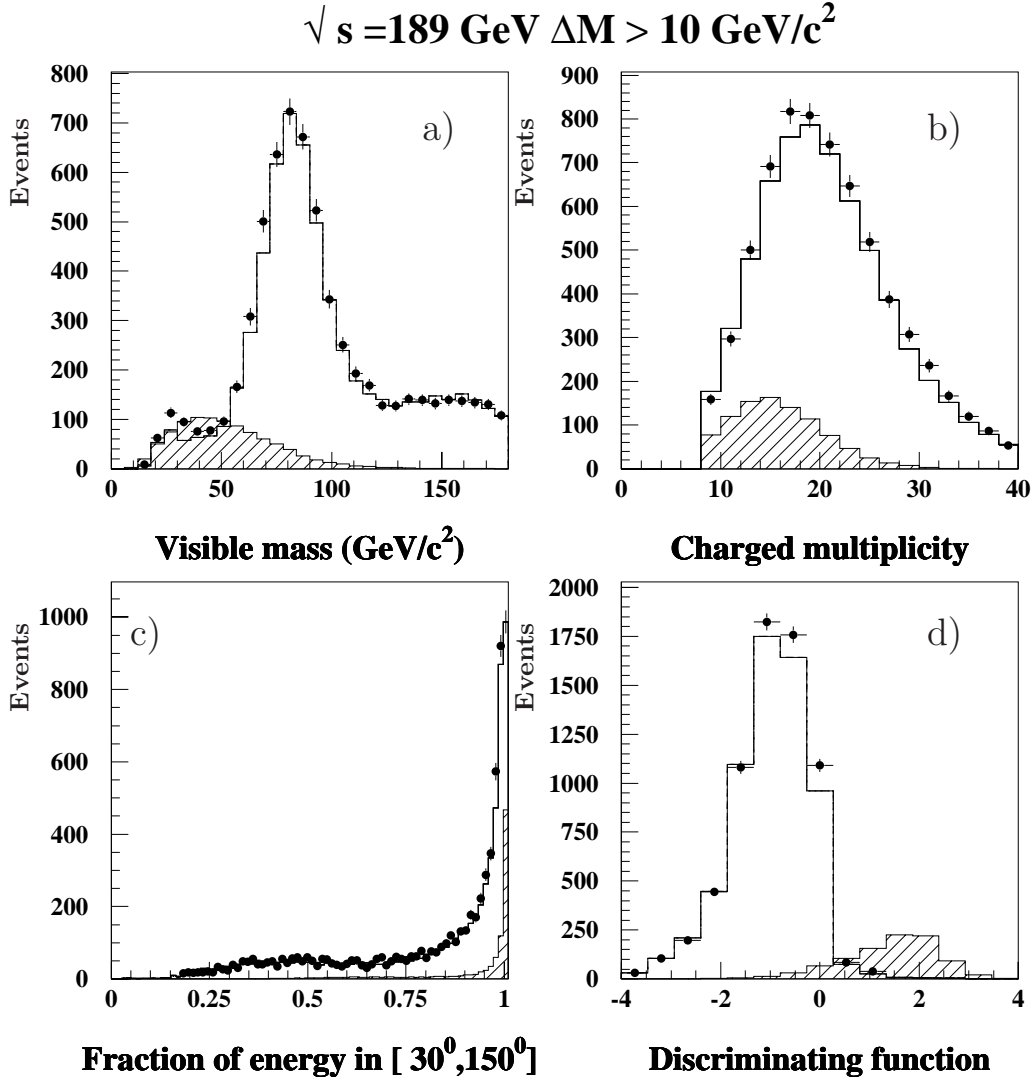


Figure 1: a) the visible mass, b) the charged multiplicity, c) the fraction of the energy in the polar angle interval $[30^\circ, 150^\circ]$ and d) the discriminating function against the $Z\gamma$ background (as described in the text) for the non-degenerate mass case concerning both stop and sbottom analysis. The dots with error bars show the data while the clear histogram is the SM prediction. Each hatched area shows the stop signal for stop masses of $70 \text{ GeV}/c^2$, $80 \text{ GeV}/c^2$ and $90 \text{ GeV}/c^2$ with $\Delta M > 10 \text{ GeV}/c^2$ (with a normalization factor to the luminosity in the range 8 to 90) where ΔM represents the mass difference between the squark and the LSP. The case $\Delta M > 10 \text{ GeV}/c^2$ corresponds to the non-degenerate mass case.

$$\sqrt{s} = 189 \text{ GeV } \Delta M \leq 10 \text{ GeV}/c^2$$

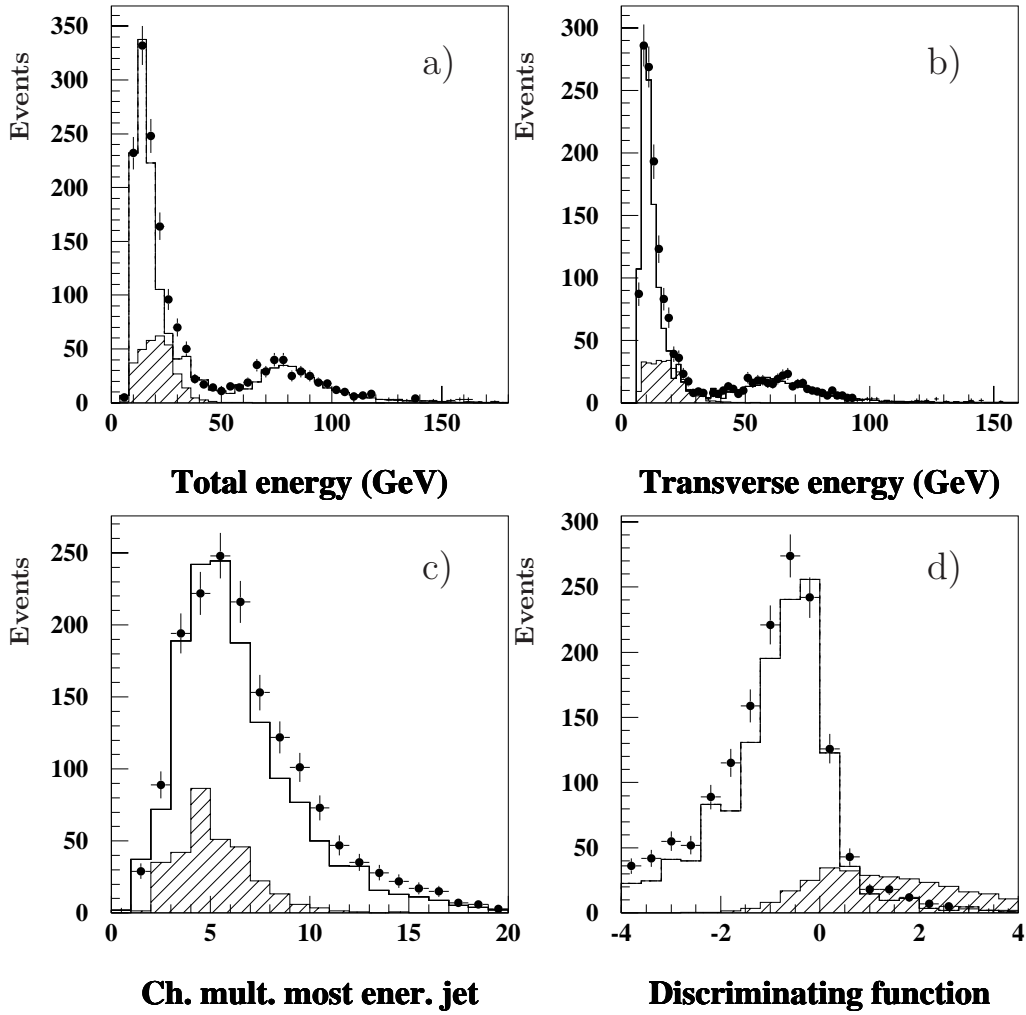


Figure 2: a) the total energy, b) the transverse energy, c) the charged multiplicity of the leading jet and d) the discriminating function (as described in the text) for the degenerate mass case of the stop analysis. The dots with error bars show the data while the clear histogram is the SM prediction. Each hatched area shows the stop signal for stop masses of $70 \text{ GeV}/c^2$, $80 \text{ GeV}/c^2$ and $90 \text{ GeV}/c^2$ with $\Delta M \leq 10 \text{ GeV}/c^2$ (with a normalization factor to the luminosity in the range 8 to 90) where ΔM represents the mass difference between the squark and the LSP. The case $\Delta M \leq 10 \text{ GeV}/c^2$ corresponds to the degenerate mass case.

$$\sqrt{s} = 189 \text{ GeV } \Delta M \leq 10 \text{ GeV}/c^2$$

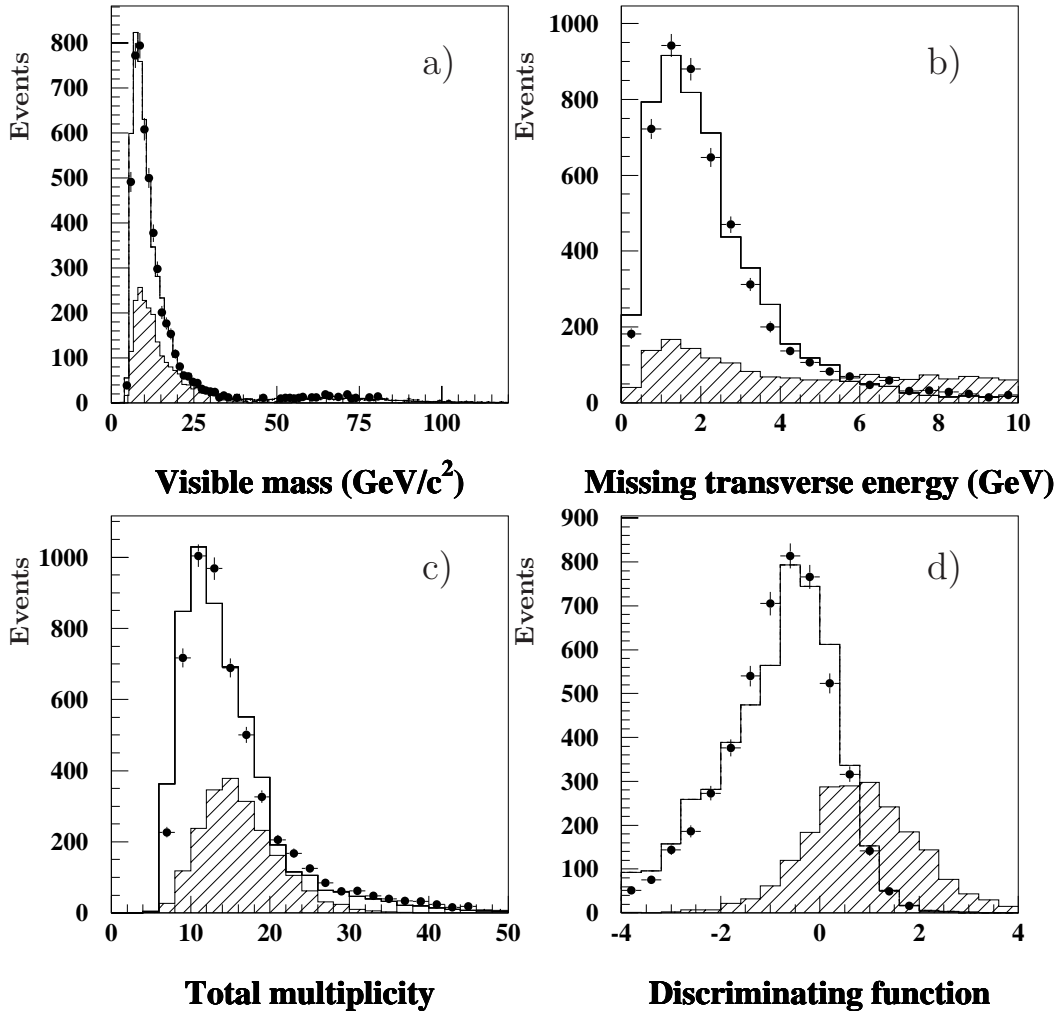



Figure 3: a) the visible mass, b) the missing transverse energy, c) the total multiplicity and d) the discriminating function (as described in the text) for the degenerate mass case of the sbottom analysis. Each hatched area shows the sbottom signal for sbottom masses of $50 \text{ GeV}/c^2$, $60 \text{ GeV}/c^2$, $70 \text{ GeV}/c^2$, $80 \text{ GeV}/c^2$ and $90 \text{ GeV}/c^2$ with $\Delta M \leq 10 \text{ GeV}/c^2$ (with a normalization factor to the luminosity in the range 5 to 100) where ΔM represents the mass difference between the squark and the LSP. The case $\Delta M \leq 10 \text{ GeV}/c^2$ corresponds to the degenerate mass case.

	DELPHI	Run: 83670	Evt: 7367
	Beam: 94.6 GeV	Proc:12-Oct-1998	
	DAS: 4-Jun-1998	Scan:17-Feb-1999	
	14:27:58	Tan+DST	

	TD	TE	TS	TK	TV	ST	PA
Act	0	0	0	31	0	0	0
	(0)	(0)	(0)	(31)	(0)	(0)	(0)
Deact	0	0	0	0	0	0	0
	(0)	(0)	(0)	(0)	(0)	(0)	(0)

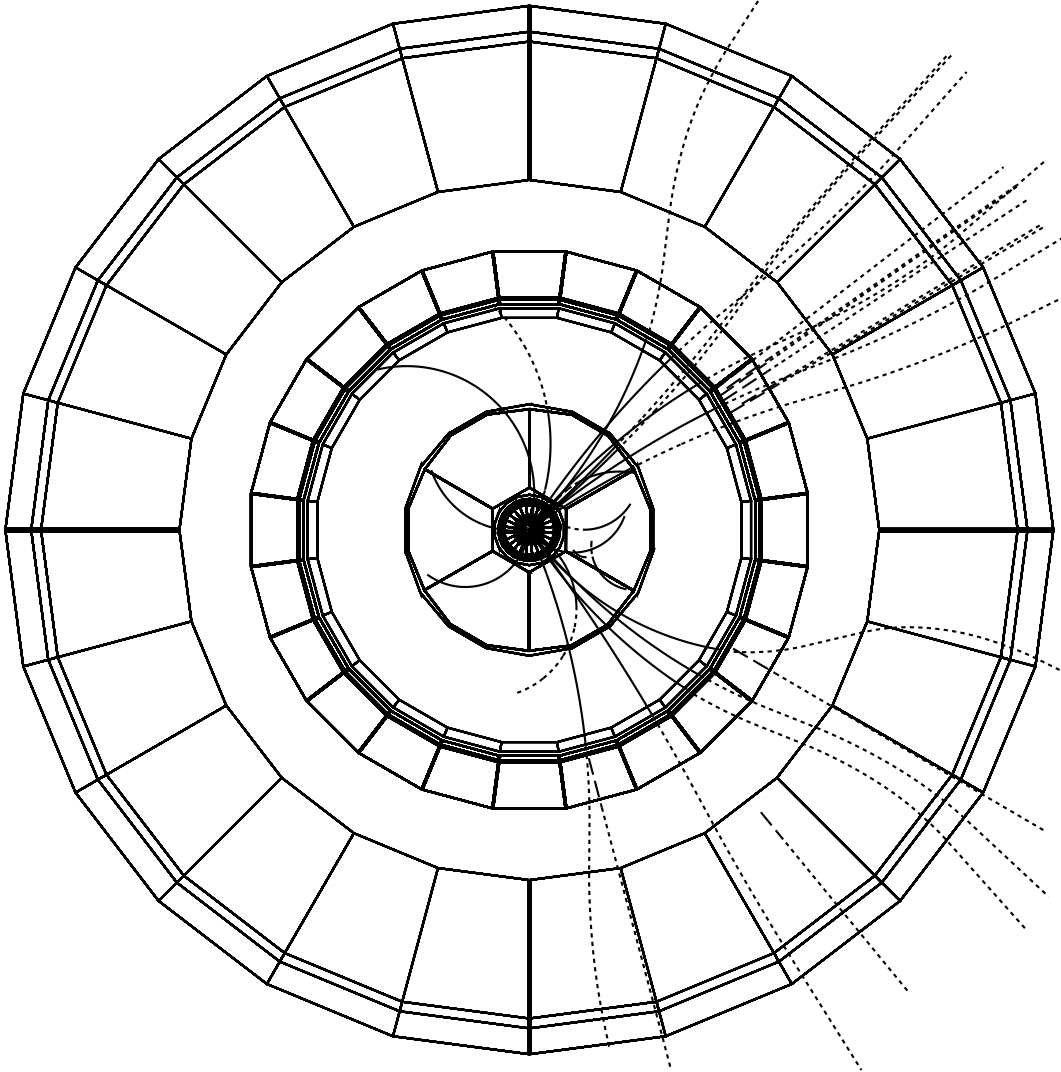


Figure 4: View of one candidate event from the non-degenerate mass case in the transverse plane. The corresponding total energy is 57.3 GeV, the charged multiplicity is found to be 27, the total visible mass is 43.3 GeV/ c^2 , the polar angle of the missing momentum is 74.8 degrees and the polar angle of the two jets are 86.5 degrees and 125 degrees respectively.

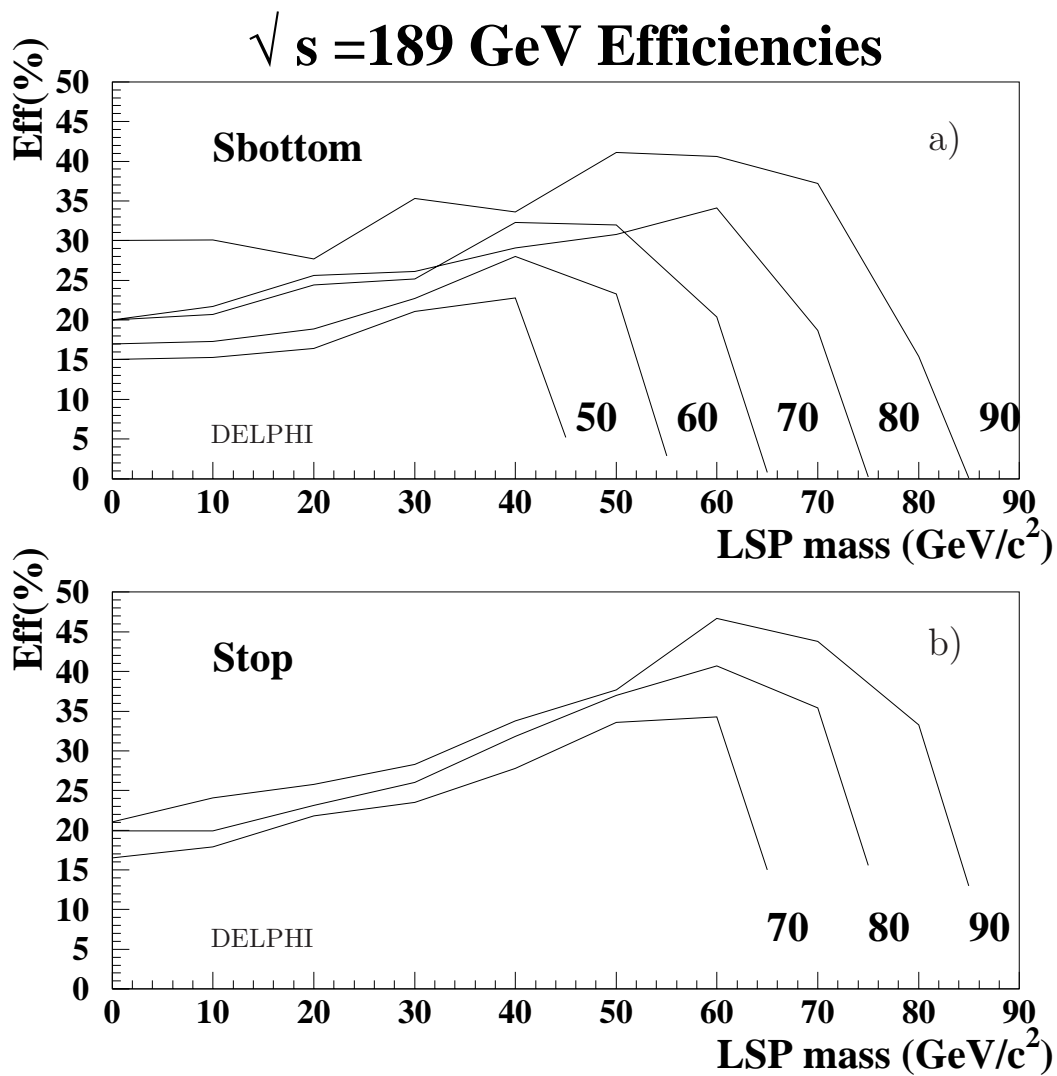


Figure 5: Efficiencies for the a) sbottom and b) stop selection in the search for two-body decays as function of the LSP mass for various sbottom and stop masses. The sbottom and stop masses are indicated on the plots in units of GeV/c^2 .

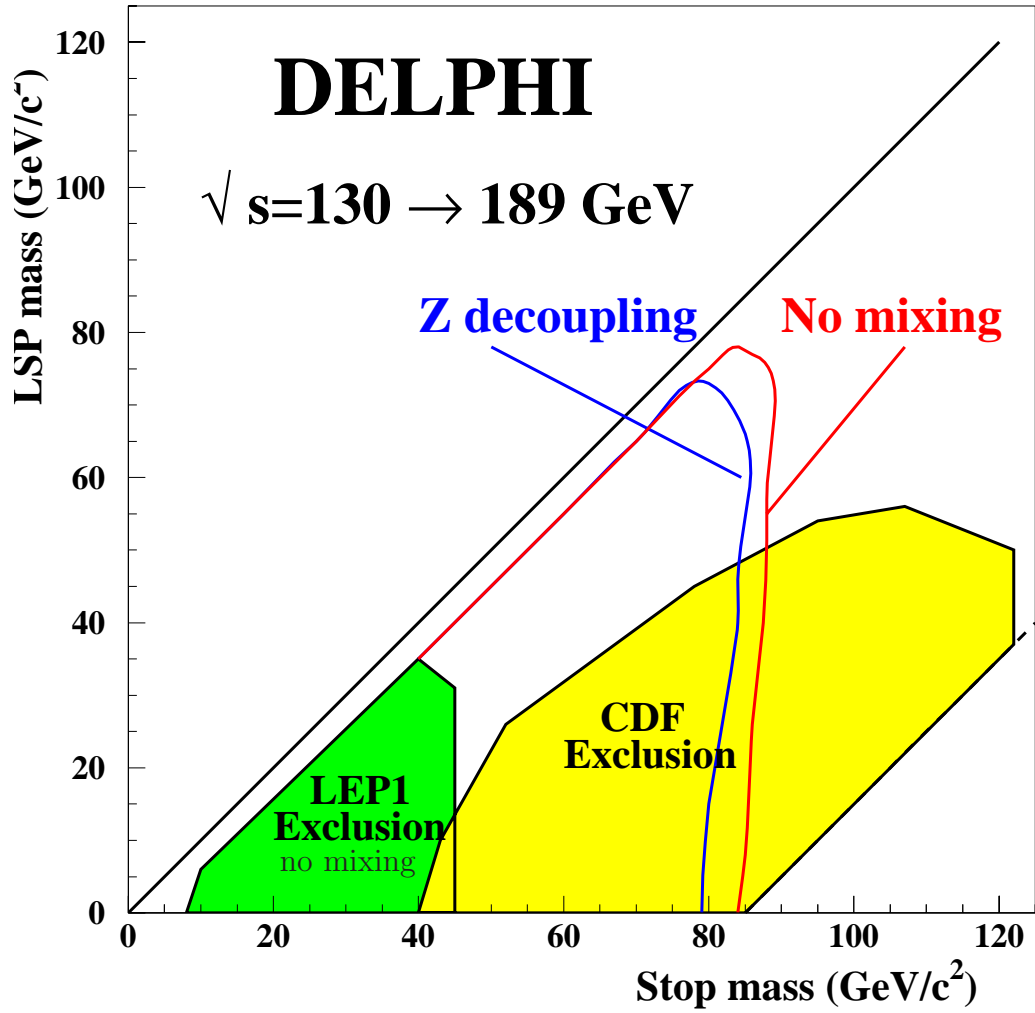


Figure 6: Exclusion domains at 95% confidence level in the $(\tilde{t}, \tilde{\chi}_1^0)$ mass plane assuming 100% branching ratio into $c\tilde{\chi}_1^0$ for pure left-handed state ($\theta = 0$ rad) and for the minimum cross-section ($\theta = 0.98$ rad) corresponding to the decoupling of the stop from the Z boson. The limits are obtained combining data at $\sqrt{s} = 130 - 189$ GeV. The shaded areas have been excluded by LEP1 [18] and CDF [19].

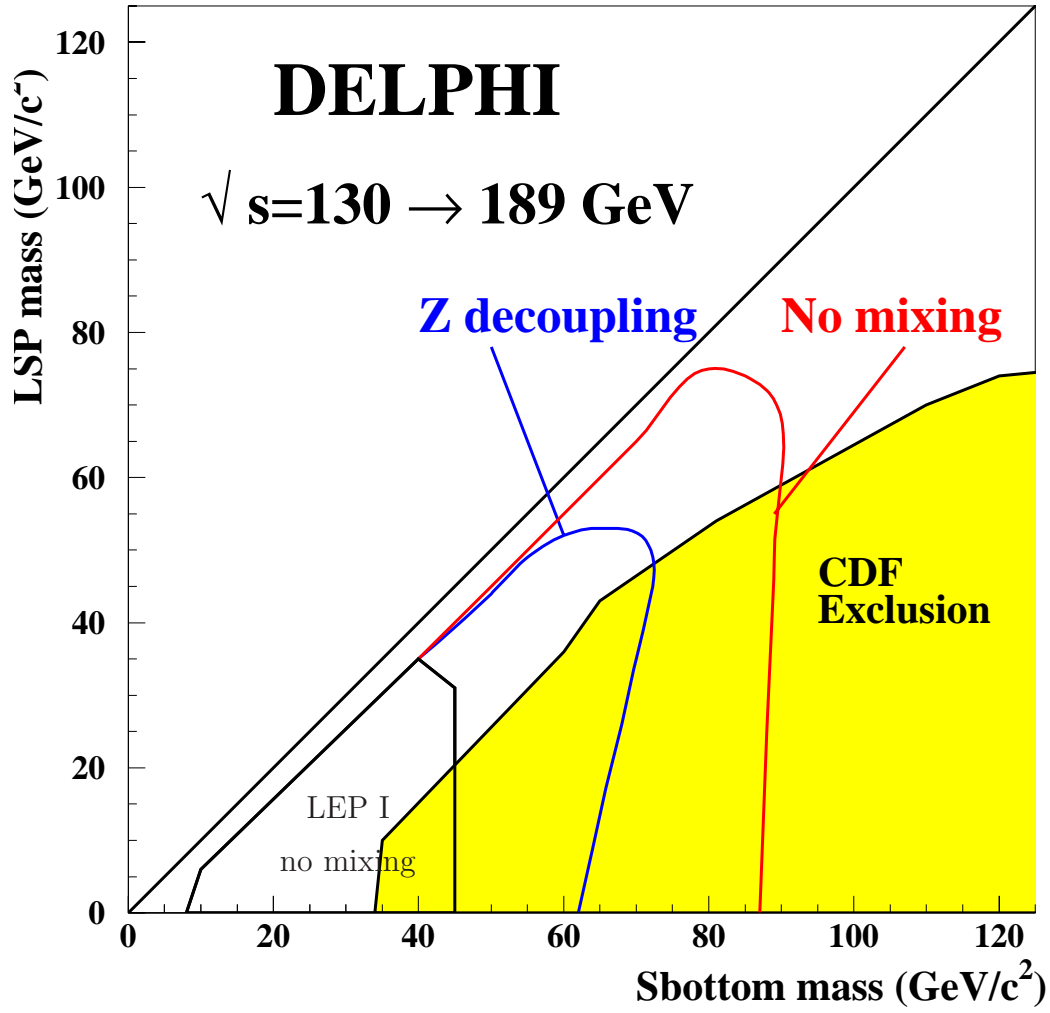


Figure 7: Exclusion domains at 95% confidence level in the $(\tilde{b}, \tilde{\chi}_1^0)$ mass plane assuming 100% branching ratio into $b\tilde{\chi}_1^0$ for pure left-handed state ($\theta = 0$ rad) and for the minimum cross-section ($\theta = 1.17$ rad) corresponding to the decoupling of the sbottom from the Z boson. The limits are obtained combining data at $\sqrt{s} = 130 - 189$ GeV.